CREEPING FLAME SPREAD ALONG FUEL CYLINDERS IN FORCED AND NATURAL FLOWS AND MICROGRAVITY

by

Michael A. Delichatsios
Fire Science and Technology Laboratory
CSIRO/DBCE
North Ryde, NSW 1670
Australia
and
Robert A. Altenkirch and Lin Tang
Department of Mechanical Engineering
Mississippi State University
Mississippi State, MS 39762, USA
and
Matthew F. Bundy
Building and Fire Research Laboratory
National Institute of Standards and Technology
Gaithersburg, MD 20899 USA
and
Subrata Bhattacharjee
Department of Mechanical Engineering
San Diego State University
San Diego, CA 92182, USA
and
Kurt Sacksteder
NASA Glenn Research Center
Cleveland, OH 44135, USA

NIST CENTENNIAL 1901-2001

NIST

National Institute of Standards and Technology
Technology Administration, U.S. Department of Commerce

CREEPING FLAME SPREAD ALONG FUEL CYLINDERS IN FORCED AND NATURAL FLOWS AND MICROGRAVITY

MICHAEL A. DELICHATSIOS,[1] ROBERT A. ALTENKIRCH,[2] MATTHEW F. BUNDY,[3]
SUBRATA BHATTACHARJEE,[4] LIN TANG[2] AND KURT SACKSTEDER[5]

[1]*Fire Science and Technology Laboratory*
CSIRO/DBCE
Fire Safety Engineering Division
North Ryde, NSW Australia 1670
[2]*NSF Engineering Research Center*
Department of Mechanical Engineering
Mississippi State University
Mississippi State, MS 39762, USA
[3]*National Institute of Standards and Technology*
Gaithersburg, MD 20899, USA
[4]*Department of Mechanical Engineering*
San Diego State University
San Diego, CA 92182, USA
[5]*NASA Glenn Research Center*
Cleveland, OH 44135, USA

Semianalytical expressions are developed for creeping flame spread parallel to a fuel cylinder axis so that spread rates measured or predicted for flat surfaces over the same material can be directly used for cylindrical surfaces. Two phenomena are identified that cause an increased flame spread rate in the cylindrical over the flat surface geometry: (1) increased heat transfer from the gas phase and (2) faster temperature increase of the solid phase. Analytical expressions from approximate solution to a conserved scalar equation are developed for the flame spread rate by simplifying the flowfield using an Oseen approximation for the opposing flow. The spread rate expression for the fuel cylinder is

$$\rho_s c_s (T_v - T_o) V_f L_{sy} \left(1 - \frac{L_{sy}}{2R_o} \right) = C(L_g/R_o) E_{FL}/\ln\left(1 + C \frac{L_s}{R_o} \right) - L_g \varepsilon \sigma (T_v^4 - T_o^4)$$

in which the terms containing the constant C account for the enhanced gas-to-surface heat transfer because of the cylindrical curvature, and those containing L_{sy}, the heated layer depth in the solid, account for a reduction in the solid volume preheated in the cylindrical compared to the flat geometry. The expression is tuned by comparison with complete numerical solutions to the flame spread problem from which the flame energy E_{FL} is determined from the flat surface geometry and the constant C chosen from heat transfer correlations. Results compare favorably with numerical solutions for cylindrical spread in forced and natural flows and microgravity and with experiments on downward flame spread on cylindrical rods in normal gravity and microgravity.

Introduction

Opposed-flow flame spread over flat surfaces, also called creeping flame spread, has been studied extensively during the past three decades [1–3]. Although the influence of parameters such as ambient oxygen content, pressure, and fuel thickness is well understood, few modeling studies exist on the effects of fuel geometry (e.g., the cylindrical geometry considered here). Ref. [4] is one exception in which radial convergence of the conduction heat flux from the gas to the solid was considered, but radiation,

important at microgravity and included here, was ignored. Fire spread in a cylindrical geometry, such as along cable insulation, is a serious fire safety concern in microgravity [5]. Previous investigations and measurements of creeping flame spread along cylindrical rods include the work of Sibulkin and Lee [6] and Fernandez-Pello and Santoro [7] at normal gravity and experiments in low gravity in the European space program [8].

The present analytical and numerical modeling was initiated in support of experiments on flame spread along cylindrical rods or tubes as part of the
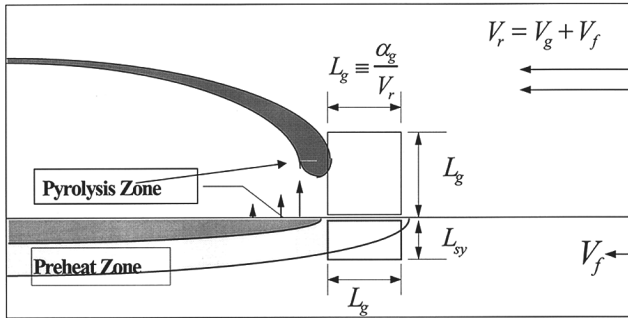
FIG. 1. Schematic of the flame spread problem.

reflight of the Solid Surface Combustion Experiment (SSCE) [9–11]. The objectives here are to (1) present the physics for creeping flame spread along a cylindrical geometry, (2) develop semianalytical expressions supported by numerical modeling that relate flame spread in the cylindrical geometry with flame spread in the flat geometry, and (3) compare predictions with existing data on cylindrical surfaces in normal gravity and microgravity [6,7,12].

Background

Review of the Flat Surface Energy Balance

Consider the control volume near the flame front shown in Fig. 1 in flame-fixed coordinates with the oxidizer approaching the flame with speed $V_r = V_g + V_f$ and the fuel approaching the flame at V_f, where V_g is the opposing flow velocity, and V_f is the spread rate. In the following discussion, the opposing flow velocity profile is flat (Oseen approximation), and gaseous thermal properties are constant, independent of temperature. A methodology to account for variable properties is outlined later. The solid is thermally thick, and the thermally thin situation is obtained as a limiting case.

The heat transfer rate per unit sample width from the flame near the leading edge expended in the sensible heating of the solid phase from ambient to the vaporization temperature (i.e., T_o to T_v) as it approaches the flame is

$$\rho_s c_s (T_v - T_o) V_f L_{sy} = E_{FL} - E_{RAD} \qquad (1)$$

The length scale in the solid phase L_{sy} is the normal depth over which the solid is preheated as it approaches the flame front where the flame heat flux extends over the gas-phase thermal length L_g, which equals a_g/V_r, with a_g the thermal diffusivity of the gas, and ρ_s and c_s the solid density and specific heat, respectively. L_{sy} equals [9]

$$\sqrt{a_s t} = \sqrt{a_s L_g / V_f}$$

whereas the axial length scale in the solid, L_{sx}, is

a_s/V_f, with t the time the solid takes to pass through the flame region of length L_g. For $L_{sy} > \tau$, the fuel thickness, the fuel is thin, and L_{sy} is replaced by τ.

The right-hand side of equation 1 contains the energy conveyed by the flame to the solid, E_{FL}, including convection and gas-phase radiation, for increasing the sensible enthalpy of the solid, reduced by the energy lost through surface reradiation, E_{RAD}, and it takes the form [13]

$$E_{FL} = \frac{h_c}{c_p} [(B - r)L] L_g = \frac{k_g}{L_g c_p}$$

$$[(B - r)L] L_g = \frac{k_g}{c_p} (B - r) L \qquad (2)$$

where the mass transfer number

$$B = [(\chi_A - \chi_R) Y_o Q_o - c_p (T_v - T_o)]/L$$

with Q_o the heat of combustion, Y_o the oxygen mass fraction, L the heat of vaporization, c_p the gas specific heat, r the stoichiometric fuel/oxidizer ratio, k_g the gas thermal conductivity, h_c the convective heat transfer coefficient, χ_A the combustion efficiency, and χ_R the radiative loss fraction. E_{RAD} is equal to the rate of heat transfer per unit width over a gaseous thermal length that also determines the region along the solid heated by the flame leading edge, that is, $E_{RAD} = q''_{rr} L_g = \varepsilon \sigma (T_v^4 - T_o^4) L_g$, with ε the surface emittance, set equal to unity here, and σ the Stefan–Boltzmann constant.

The energy balance of equation 1, equivalent to the de Ris expression except for a constant [14], together with the definitions for L_g, L_{sy}, E_{FL}, and E_{RAD} allow the flame spread rate to be determined. The formulation can also be generalized for different profiles of opposing flow by noting that the flame spread rate can be interpreted to depend on two parameters: the flame energy, E_{FL}, and the gaseous thermal length, L_g.

There are, for all intents and purposes, three spread rate regimes: (1) a thermal regime at moderate opposing flow velocity in which radiation is unimportant, and the flame energy becomes a property of the material and its environment, independent of L_g for a thin fuel; (2) a high opposing flow velocity

regime in which radiation is unimportant, but E_{FL} depends on a Damköhler number and hence L_g, even for a thin fuel, and the shape of the velocity profile; and (3) a low opposing flow velocity regime in which E_{FL} depends on L_g, at least to an extent, through the dependence of the radiation on L_g. As $V_g \to 0$ in the quiescent microgravity environment (i.e., the limiting case of the low opposing flow velocity regime), V_f is the only velocity that appears, and E_{FL} depends primarily on material and environmental properties. With the exception of the high opposing flow velocity regime, we can view E_{FL} as a material property that may be determined by measurement [13] or from numerically determined spread rates in conjunction with equation 1 accounting for variable properties and the opposing flow velocity profile, which contributes to determining h_c.

Effects of Cylindrical Geometry

Application of equation 1 can be extended to creeping flame spread along a cylinder by emphasizing the similarities and differences between the flat and cylindrical geometry with the same opposing flow velocity:

1. The gaseous length scale, L_g, remains the same.
2. The flame energy transferred to the solid increases because the heat transfer coefficient, h_c, increases with the curvature [4,15].
3. The sensible heat required to raise the solid surface temperature from ambient to the pyrolysis value decreases compared to a flat surface of the same thickness as the radius because the cylindrical surface seen by the flame is convex.

Model Development

Flame Energy in the Cylindrical Geometry

It is well known that heat fluxes in laminar flow along a cylinder increase as the radius decreases (see Ref. [15] for the hot cylinder and Ref. [16] for burning along a cylinder). Therefore, the heat transfer rate near the leading edge also increases as the cylinder radius decreases. A simple expression is developed to evaluate the increased heat flux, for phenomena 2 and 3 above, by comparison to the heat flux on a flat plate.

We start with an Oseen-type opposing flow having a uniform velocity profile and constant properties following development for creeping flame spread on a flat plate [13,14,17]. The equation in cylindrical coordinates for a conserved scalar, ϕ_s in the gaseous flow is

$$V_r \frac{\partial \phi}{\partial x} = a_g \left(\frac{\partial^2 \phi}{\partial x^2} + \frac{1}{r} \frac{\partial}{\partial r} \left(r \frac{\partial \phi}{\partial r} \right) \right) \quad (3)$$

where x and r are the axial and radial coordinates,

respectively. Recall that V_r is a relative velocity into the flame and not a radial velocity. A methodology to calculate the spread rate along the cylinder in a manner similar to the flat geometry [18] is difficult to implement because Bessel functions are needed when taking the Fourier transform, applying Wiener–Hopf splitting, and, finally, inverting the results. Instead, we evaluate modification of the heat transfer rate to the cylinder because of curvature by using the parabolic form of equation 3 away from the leading edge such that we neglect axial diffusion, which is accounted for in equation 1. Parabolic equations have been used before in the flame spread problem and have been found to give a proper account of energy redistribution in the gas and solid and a spread rate equivalent to the elliptic problem [4,17].

The boundary conditions are that ϕ has a constant value at the cylinder surface, $\phi = \phi_c$, and is zero at infinity. A closed-form solution can be found in this case [19] (example 7-18), which in terms of the present formulation is

$$\frac{\phi(r, x)}{\phi_c} = 1 + \frac{2}{\pi} \int_0^\infty e^{-(\delta_v/R_o)^2 \omega^2}$$

$$\frac{J_o(\omega r/R_o)Y_o(\omega) - J_o(\omega)Y_o(\omega r/R_o)}{\omega[J_o^2(\omega) + Y_o^2(\omega)]} \, d\omega \quad (4)$$

Here, J_o and Y_o are Bessel functions, with R_o the cylinder radius, and the thermal length, δ_v, is $\sqrt{a_g x/V_r}$. The derivative of equation 4 at the cylinder surface, proportional to the heat flux, takes the form

$$\frac{\partial \phi}{\partial r} (\text{at } r = R_o) = \frac{\phi_c}{\delta_v} \frac{2\delta_v}{\pi R_o} \int_0^\infty e^{-(\delta_v/R_o)^2 \omega^2}$$

$$\frac{2}{\pi \omega[J_o^2(\omega) + Y_o^2(\omega)]} \, d\omega \quad (5)$$

where standard properties of the Bessel functions have been used.

An approximate, analytical expression for this integral that is useful in developing a closed-form energy balance for the cylinder similar to equation 1 for the flat surface can be derived after finding its asymptotic expressions for small and large δ_v/R_o. For large radius (i.e., the flat plate), the integral equals $\sqrt{\pi R_o/2\delta_v}$ because $2/\{\pi\omega[J_o^2(\omega) + Y_o^2(\omega)]\} = 1$ for large values of the argument, which mostly contribute to the integral. For small radius, the integral equals

$$\frac{\pi}{2} \int_0^\infty e^{-(\delta_v/R_o)^2 \omega^2} \frac{1}{\omega^2 [\ln(\omega/2)]^2} \, d\omega$$

which, following partial integration, is approximately $\pi/[2 \ln(2\delta_v/R_o)]$.

An approximation of the heat flux for any radius can be determined by combining the previous approximations and checking with numerical integration of equation 5, which gives

$$\frac{\left(\frac{\partial \phi}{\partial r}\right)_{r=R_\mathrm{o}}}{\left(\frac{\partial \phi}{\partial r}\right)_{r=\infty}} = \frac{\sqrt{\pi}\,\frac{\delta_\mathrm{v}}{R_\mathrm{o}}}{\ln\left(1 + \sqrt{\pi}\,\frac{\delta_\mathrm{v}}{R_\mathrm{o}}\right)} \qquad (6)$$

This expression, accurate for the Oseen-constant-property flow, is useful in correlating experimental or numerical data. The coefficient $C = \pi^{1/2}$ here and the length δ_v will depend on the particular boundary layer flow along the cylinder, including laminar combustion.

Heat Conduction into the Cylinder

Flame spread occurs along the cylinder because the cylinder is preheated by the flame leading edge. The sensible heat can be found by solving the problem for heat conduction into a cylinder for a constant heat flux over a specified preheating time. An approximation for this preheating energy can be derived from the exact solution in Ref. [20] (p. 194). For the present situation, the energy conducted into the cylinder for preheating takes the form

$$\rho_s c_s (T_\mathrm{v} - T_\mathrm{o}) V_\mathrm{f} L_\mathrm{sy} \left(1 - \frac{L_\mathrm{sy}}{2R_\mathrm{o}}\right)$$

Coupling with equation 6, the flame spread equation along a cylinder becomes

$$\rho_s c_s (T_\mathrm{v} - T_\mathrm{o}) V_\mathrm{f} L_\mathrm{sy} \left(1 - \frac{L_\mathrm{sy}}{2R_\mathrm{o}}\right)$$

$$= \frac{C\,\frac{L_\mathrm{g}}{R_\mathrm{o}}}{\ln\left(1 + C\,\frac{L_\mathrm{g}}{R_\mathrm{o}}\right)}\, E_\mathrm{FL} - E_\mathrm{RAD} \qquad (7)$$

For L_sy greater than or equal to R_o, the cylinder is thermally thin, in which case $L_\mathrm{sy} = R_\mathrm{o}$.

Applications

For a cylinder at a fixed temperature, the numerical results for augmentation of the heat flux can be correlated for constant properties for several situations [15]. For a forced boundary layer flow along the cylinder surface, in the parabolic region of the flow removed from the leading edge of the cylinder

$$\frac{Nu(R_\mathrm{o})}{Nu(\mathrm{flat})} = \frac{3.21\,\frac{\delta_\mathrm{v}}{R_\mathrm{o}}}{\ln\left(1 + 3.21\,\frac{\delta_\mathrm{v}}{R_\mathrm{o}}\right)}$$

with Nu the local Nusselt number, δ_v defined as before, and $Pr = 0.7$. For the natural convection case, again in the parabolic region, the constant 3.21 in

the expression for forced flow is replaced by 1.80, and the boundary layer thickness is

$$\delta_\mathrm{v} = \left(\frac{a_\mathrm{g} x}{\sqrt{g[(T_\mathrm{w}/T_\mathrm{o}) - 1]x}}\right)^{1/2}$$

where T_w is the wall temperature, and g is the acceleration of gravity. The difference in the constant C for the Oseen flow ($\sqrt{\pi}$), the forced flow (3.21), and the natural convection flow (1.80) is due to the different temperature profiles, which also alter the definition of the thermal length δ_v. From these results, we see that the form of equation 6 reproduces well the data concerning the augmentation of the heat fluxes from the gas to the solid because of the cylindrical curvature.

Flame Spread on Cylinders

The major application of this work is flame spread along cylindrical surfaces. We use numerical modeling results from both steady and unsteady computational codes [11,12,21]. In the numerical model, the Navier–Stokes equations are solved, including single-step Arrhenius gas-phase combustion and surface pyrolysis. Surface re-radiation and detailed gas-phase radiation, including feedback to the fuel surface, are accounted for by employing an overall Planck mean absorption coefficient in the gas obtained from an overall energy balance consistent with solution to the radiative transfer equation [12]. Additionally, experimental spread rate measurements from the SSCE for spread along cylindrical fuel samples in the quiescent microgravity environment of the space shuttle are quoted later [10,12]. The reader is referred to Refs. [11], [12], and [21] for details concerning the numerical model and properties employed and to Refs. [10] and [12] for a detailed description of the experimental configuration. All results here are for polymethylmethacrylate (PMMA) as the fuel.

To apply equations 1 and 7, E_FL and a_g are needed. For the flat surface, we notice that the thin fuel E_FL is independent of gas-phase properties such that it can be determined from solid properties, $\rho_s = 1190$ kg/m^3, $c_s = 1465$ J/kg · K, $T_\mathrm{v} = 640$ K, once V_f is known, for which we use results from the numerical model. With E_FL known, the gas-phase thermal diffusivity that appears in L_sy can be determined from the flat surface, thick fuel limit, using, again, the thick limit spread rate from numerical modeling. Obviously, experimental values for the V_f values may be used as well to determine E_FL and a_g.

For a PMMA, thermally thin fuel thickness τ of 0.1 mm, and using equation 1 with $L_\mathrm{sy} = \tau$ in an opposing, forced flow of 40 cm/s at 1 atm, we get that E_FL is 127, 305, 404, and 522 W/m for oxygen mass factions in nitrogen of 0.233, 0.533, 0.727, and 1.0, respectively. The corresponding spread rates are
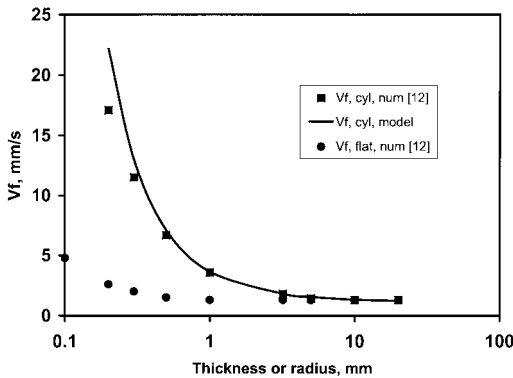
FIG. 2. Flame spread rate over PMMA flat surfaces and cylinders for $Y_o = 0.533$ in N_2 at 1 atm and a forced, opposing flow of 40 cm/s as a function of thickness or radius, including numerical computations and the analytical model for cylinders from equation 7. Squares, numerical computations for cylinders from Ref. [12]; circles, numerical computations for flat surfaces from Ref. [12]; solid line, model equation for cylinders.

2.15, 5.14, 6.81, and 8.80 mm/s, respectively [21]. Because E_{FL} is directly related to the flame temperature, the ratio of the E_{FL} values at different oxygen mass fractions is approximately the ratio of the corresponding oxygen mass fractions.

Corresponding thick limit spread rates for the same oxygen mass fractions are, in ascending mass fraction order, 0.185, 1.18, 1.85, and 3.42 mm/s. These spread rates may be used to determine a_g from the thick formulation of equation 1, and then E_{FL} and a_g are known for application of equation 7 at a particular oxygen concentration, presuming C can be selected.

The determination of a_g that appears in L_{sy} is complicated by the fact that the correct velocity to use for V_g is an equivalent velocity at a distance L_g from the surface that with L_g describes the velocity gradient at the surface rather than the free stream velocity because of the effect of the velocity profile on distances over which heat can be conducted [22]. The free stream velocity is always higher than the equivalent velocity; a_g then is an effective property such that the ratio of a_g/V_g is identical to the actual thermal diffusivity divided by the equivalent velocity. Using the listed thick limit spread rates, and equation 1, we get an a_g of about 8.80×10^{-4} m^2/s as an average for all the oxygen mass fractions. The equivalent velocity for this configuration, from Ref. [22], is about 7 cm/s or about 6 times smaller than V_g so that the actual thermal diffusivity is around 1.5×10^{-4} m^2/s. The higher value is equivalent to a thermal diffusivity for 1 atm at approximately 2400 K, while the lower value is for approximately 950 K, a more realistic temperature for property evaluation

[22]. However, as long as V_g and a_g are used consistently in determining L_{sy}, the result is accurate.

Because of the enhanced heat transfer from the gas to the solid because of the curvature, a_g also appears in the term CL_g/R_o. This a_g, however, need not be the same as the one used for L_{sy}, which appears in equation 7 as a result of in-depth heating. It is the product Ca_g in the curvature effect that is important rather than a_g alone, so that once V_g and C are selected, a_g for use in CL_g/R_o can be determined by requiring the thick limit, steady spread rate, if it exists, to be recovered.

Forced Flow

In Fig. 2, numerical spread rate results are presented comparing the flat and cylindrical geometry as a function of fuel thickness and comparing the numerical computations to the analytical model from equation 7, which represents the behavior well for the cylindrical fuel. Spread rates for the cylinder are, as expected, higher than for the flat surface as the thickness decreases to the thin limit.

For Fig. 2, we determined an a_g of 1.7×10^{-4} m^2/s for use in CL_g/R_o. With the equivalent velocity being about 6 times smaller than V_g, the actual a_g for use in CL_g/R_o would be about 30×10^{-6} m^2/s, which is equivalent to a temperature of about 350 K, which is realistic for determination of heat conduction into the ambient oxidizer. Although the value of C used derives from a boundary layer configuration, the flame in a forced flow is embedded in the boundary layer, and the factor in front of E_{FL} is to account for the effect of curvature on heat transfer to the surface rather than upstream heat transfer, which is accounted for in the energy balance itself through E_{FL} and L_g.

Figure 3 shows numerical computation and analytical model equation results for spread rate as a function of opposing, forced flow in the absence of gravity for a fixed cylinder diameter of 3.2 mm, the diameter used in the SSCE, using the same model equation deriving from equation 7 as for Fig. 2. The model does not reproduce the computed spread rates as well as it does as a function of radius for a fixed velocity. The reason is that once the model parameters are set for a fixed velocity, the behavior of V_f as a function of radius is accurately described by the model equation, but as the velocity changes, the model becomes less accurate because the free stream velocity should be replaced by the equivalent velocity for accurate representation [22]. At the lowest velocities, around 5 cm/s, the behavior of the model and computed spread rates becomes dissimilar. The reason for the upturn in spread rate in the model is that $C(L_g/R_o)/\ln(1 + CL_g/R_o)$ becomes large for large L_g/R_o, while $L_{sy}(1 - L_{sy}/2R_o)$ is bounded, so a significant increase in the curvature affecting the heat transfer from the gas to the solid is obtained. The computational results do not show
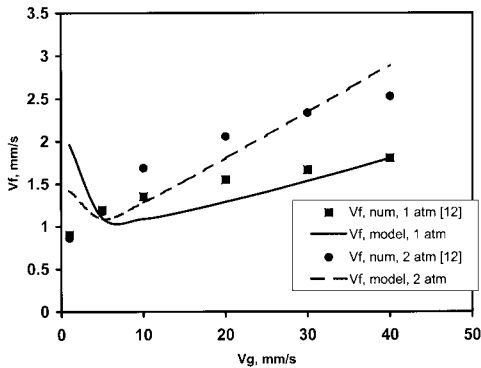
FIG. 3. Forced flow, microgravity flame spread rate over PMMA cylinders for $Y_o = 0.533$ in N_2 at 1 atm and $R_o = 3.2$ mm as a function of opposing flow, including numerical computations and the analytical model from equation 7. Squares, numerical computations for 1 atm from Ref. [12]; solid line, model equation for 1 atm; circles, numerical computations for 2 atm from Ref. [12]; dashed line, model equation for 2 atm.
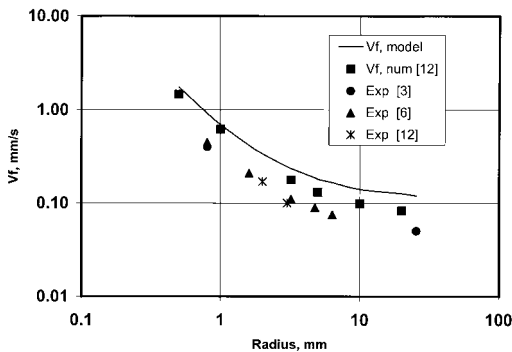

FIG. 4. Downward flame spread rates over PMMA cylinders in air at 1 atm as a function of radius, including numerical computations, the analytical model from equation 7, and experiment. Solid line, model equation; squares, numerical computations from Ref. [12]; circles, experiment [3]; triangles, experiment [6]; asterisks, experiment [12].

the upturn because of the effects of radiation depressing the heat transfer to the solid and decreasing the gas-phase thermal length scale [11].

Natural Convection

Application of the model equation in natural convection requires selection of a velocity induced by the spreading flame, which is $(g_g g E_{FL}/k_g T_o)^{1/3}$ [23]. Using the same properties as for the forced flow, selecting the thermal conductivity of the gas k_g at approximately the same temperature as the a_g used in CL_g/R_o in forced flow, and using $C = 1.80$ from

natural convection, we get the results shown in Fig. 4 for spread rate as a function of radius for downward spread on cylinders comparing numerical model results with experiment and the model equation. The model equation describes the V_f versus R_o behavior correctly, although the V_f values tend to be higher than either numerical or experimental results, mostly due to the approximate nature of the velocity selected.

Microgravity

In quiescent microgravity, steady spread occurs only for thin fuels [11], and so in application of equations 1 and 7, L_{sy} is the fuel thickness or radius. Additionally in microgravity, radiation from the gas is significant and, in fact, is the cause for the occurrence of only unsteady spread to extinction for thick fuels [11], and so E_{FL} is lower than the values quoted above and must be redetermined. Fig. 5 shows numerically determined spread rates for flat surfaces at 1 and 2 atm as well as the model equation, equation 1, and numerically determined spread rates for cylinders at 2 atm, along with model results from equation 7 as well as measured spread rates from the SSCE at 1 atm. The computational data stop at a thickness beyond which there is no steady spread. Spread rates for cylinders are higher than for flat surfaces, and the cylinders are able to maintain steady spread for a larger thickness because of the enhanced heat transfer that occurs as a result of the curvature. Pressure effects for the cylinder appear to be minimal. The behavior of the spread rate for the cylinders is adequately described by the model equation with $C = 3.21$ from the forced flow configuration.

In application of the model equations to quiescent microgravity, E_{FL} was determined to be 164 W/m for the 0.533 mass fraction of oxygen in nitrogen at 1 atm (compared to 305 W/m in normal gravity) and 255 W/m at 2 atm. These values were obtained using the flat surface numerically determined spread rates for the thinnest fuel of Fig. 5, where the spread rates are highest and the effects of surface radiation the least. E_{FL} in normal gravity is effectively independent of pressure, while in microgravity it depends on pressure because of the decrease in total flame heat loss by radiation with increasing pressure. Although absorption coefficients increase with increasing pressure, the decrease in length scale of the flame results in the reduced radiation loss with increasing pressure [24]. E_{FL} also depends slightly on fuel thickness as a result of increased flame radiation loss with decreasing V_f.

Because there is no steady thermally thick spread in quiescent microgravity, a_g only appears in the CL_g/R_o terms. In constructing Fig. 5, a_g was set
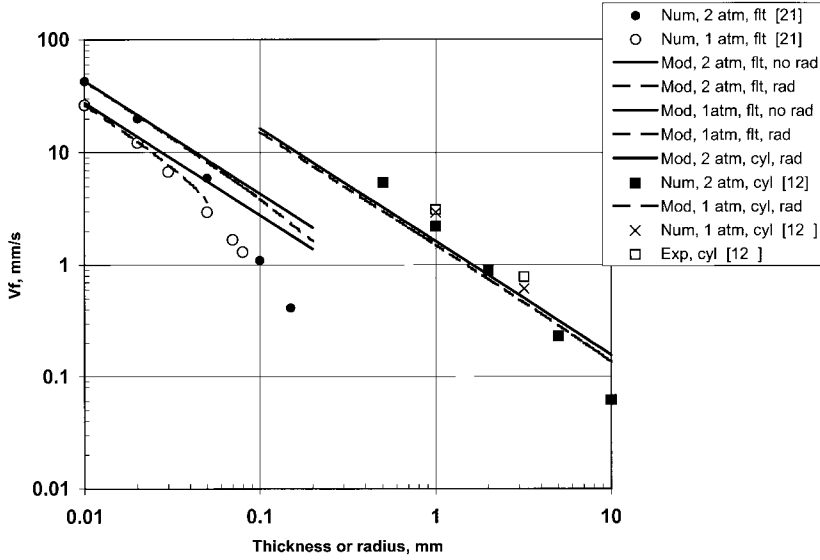
FIG. 5. Quiescent microgravity flame spread rates for $Y_o = 0.533$ in N_2 at 1 atm as a function of thickness or radius, including numerical computations, the analytical models for flat surfaces and cylinders, and experiment. For flat surfaces (to the left): closed circles, numerical computations for 2 atm from Ref. [21]; open circles, numerical computations for 1 atm from Ref. [21]; solid lines, model equation for 2 atm, no radiation; dashed line, model equation for 2 atm, including radiation; solid line, model equation for 1 atm, no radiation; dashed line, model equation for 1 atm, including radiation. For cylinders (to the right): solid line, model equation for 2 atm, including radiation; closed squares, numerical computations for 2 atm from Ref. [12]; dashed line, model equation for 1 atm, including radiation; ✕, numerical computations for 1 atm from Ref. [12]; closed squares, experiment [12].

equal to a value for ambient temperature, which reduces L_g compared to its normal gravity counterpart to account for the fact that radiation causes a depression in the length scale such that the mass and thermal diffusion scales are similar so that steady spread can be maintained. When the mass diffusion scale is large compared to the thermal diffusion scale, steady spread is not possible [11].

An additional experiment executed in the SSCE employed a hollow cylinder of 3.2 mm radius and 1 mm wall thickness. The model equation for cylindrical spread gives a hollow cylinder spread rate approximately 1.54 times the solid cylinder of the same radius, 0.71 mm/s compared to 0.46 mm/s. The ratio of numerically determined spread rates is 1.36, 0.83 mm/s compared to 0.61 mm/s, and the measured ratio from the SSCE is 1.19, 0.93 mm/s compared to 0.78 mm/s. The model and numerical results overpredict somewhat the curvature effect for the hollow sample. In the model equation, gas curvature (the multiplier before E_{FL}) and radiation (through E_{FL} and E_{RAD}) are accounted for separately when, actually, they are not separate. Radiation reduces L_g [24], which reduces the curvature effect. This coupling of gas curvature and radiation accounted for computationally but not in the model equation results in overprediction of the curvature effect from the model being the largest.

Conclusions

Flame spread rates along cylinders are higher than those over flat surfaces of the same thickness in all configurations investigated, that is, forced and natural convection flows and microgravity. Analytical modeling shows that for the cylindrical geometry, there is an enhancement of the heat transfer from the flame to the fuel to drive the spreading flame because of the fuel curvature, and the rate of temperature rise of the solid is faster because there is less material within the cylinder per unit length around the cylinder that needs to be heated than for the flat surface. The former phenomenon increases the spread rate by a factor of

$$C(L_g/R_o)/\ln\left(1 + C\,\frac{L_g}{R_o}\right)$$

above that of the flat surface, and the latter reduces the heated layer depth in the cylinder and increases the spread rate by a factor $(1 - L_{sy}/2R_o)^{-1}$. For the thin cylinder with $L_{sy} = R_o$, this factor is two such that the cylindrical spread rate is at least twice that for the flat surface. E_{FL} is obtainable from numerical simulation or from measurement for thin fuels and may be thought of as a material property, particularly when flame radiation is not important.

Analytical expressions for cylindrical spread derived from approximate solution to the scalar conservation equation that include the factors mentioned above describe the behavior of the spread rate as a function of cylinder radius well for forced and natural flows and quiescent microgravity. Spread rate variations with flow velocity are harder to match with the analytical expressions because of the influence of the characteristic velocity gradient on the appropriate velocity to use in the formulation.

REFERENCES

1. Di Blasi, C., and Continnillo, G., *Combust. Sci. Technol.* 54:25–36 (1987).

2. Bhattacharjee, S., and Altenkirch, R. A., *Proc. Combust. Inst.* 23:1627–1633 (1991).

3. Fernandez-Pello, A. C., and Hirano, T., *Combust. Sci. Technol.* 32:1–31 (1983).

4. Higuera, F. J., and Liñán, A., *Combust. Theory Modelling* 3:259–265 (1999).

5. National Aeronautics and Space Administration, *Fire Safety in Extraterrestrial Environments,* NASA/TM-1998-207417 (1998).

6. Sibulkiin, M., and Lee, C. K., *Combust. Sci. Technol.* 9:137–147 (1974).

7. Fernandez-Pello, A. C., and Santoro, R. J., *Proc. Combust. Inst.* 17:1201–1209 (1979).

8. Tarifa, C. S., Liñán, A., Salva, J. J., Juste, G. L., Tizon, J. M., and Cura, J. M., *Study on Combustion Processes in Reduced Gravity,* final ESA report LP Tr 9004, 1990.

9. West, J., Tang, L., Altenkirch, R. A., Bhattacharjee, S., Sacksteder, K., and Delichatsios, M. A., *Proc. Combust. Inst.* 26:1335–1343 (1996).

10. Altenkirch, R. A., Tang, L., Bhattacharjee, S., Bundy, M. F., Sacksteder, K., and Delichatsios, M. A., "Reflight of the Solid Surface Combustion Experiment: Flame Radiation Near Extinction," in *Fifth International Microgravity Combustion Workshop,* NASA/CP-1999-2089 17:27–30 (1999).

11. Altenkirch, R. A., Tang, L., Sacksteder, K., Bhattacharjee, S., and Delichatsios, M. A., *Proc. Combust. Inst.* 27:2515–2524 (1998).

12. Bundy, M. F., "A Computational Model for Flame Spread along Cylindrical Fuels in a Microgravity Environment," Ph.D. dissertation, Washington State University, Pullman, WA, 1998.

13. Delichatsios, M. A., *Proc. Combust. Inst.* 26:1495–1503 (1996).

14. De Ris, J. N., *Proc. Combust. Inst.* 12:241–252 (1969).

15. Wang, T.-Y., and Kleinstreuer, C., *J. Heat Transfer* 111:393–398 (1989).

16. Lyu, H.-Y., and Chen, L.-D., *Combust. Flame* 87:169–181 (1991).

17. Wichman, I. S., and Williams, F. A., *Combust. Sci. Technol.* 32:91–123 (1983).

18. Delichatsios, M. A., *Combust. Sci. Technol.* 44:257–267 (1981).

19. Arpaci, V. S., *Conduction Heat Transfer,* Addison-Wesley, Reading, MA, 1966.

20. Luikov, A. V., *Analytical Diffusion Theory,* Academic Press, New York, 1968.

21. West, J., "Forced Opposed Flow Flame Spread over Flat Solid Fuels in the Thermal, Near Quiescent and Chemical Kinetic Regime," Ph.D. thesis, San Diego State University/University of California, San Diego, 1997.

22. Bhattacharjee, S., West, J., and Altenkirch, R. A., *Proc. Combust. Inst.* 26:1477–1485 (1996).

23. Altenkirch, R. A., Eichhorn, R., and Shang, P. C., *Combust. Flame* 37:71–83 (1980).

24. Bhattacharjee, S., Altenkirch, R. A., Olson, S. L., and Sotos, R. G., *J. Heat Transfer* 113:670–676 (1991).